Optimization of Class–2 Tensegrity Towers

Milenko Masic and Robert E. Skelton,

Mechanical and Aerospace Engineering Department, Structural Systems & Control Lab,
University of California San Diego, 9500 Gilman Drive, La Jolla, CA 92093-0411

ABSTRACT

This paper concerns the optimal mass–to–stiffness ratio design of class–2 tensegrity towers. For different loading scenarios, the procedure seeks the topology and geometry of the structure that yields an optimal design satisfying common constraints. The domain of feasible tensegrity geometries is defined by imposing tensegrity equilibrium conditions on both unloaded and loaded structure. Remaining constraints include strength constraints for all elements of the structure and buckling constraints for bars. The symmetry of the design is imposed by restricting the domain of geometric variables and element parameters. The static response of the structure is computed by using a nonlinear large displacement model. The problem is cast in the form of a nonlinear program. The influence of material parameters on the optimal shape of the structure is investigated.

Keywords: Tensegrity, Optimal stiffness, Geometry, Design constraints, Nonlinear program

1. INTRODUCTION

A tensegrity structure is a prestressable stable truss-like system. Unlike regular trusses, tensegrities involve string elements that are capable of transmitting loads in one direction only. Admissible connections between elements are ball joints. External loads can only act at the joints so that no torque can be applied on the elements. Increased interest in tensegrity structures is a result of their favorable properties. All elements of the structure are loaded axially only. This type of load can be more efficiently carried than bending loads.

Tensegrity structures enable the integration of several functions within a same element, [1]. String elements, that are load carrying members, can also serv the control function, [2]. The choice of materials and element geometry can be specialized for axial loads, and split further in materials optimized for compressive and tensile stresses and strains.

Tensegrity technology thus far is characterized by the existence of successful dynamic models, e.g. [3] and control strategies, e.g [2], [4–9]. A significant amount of research has been invested in different tensegrity form-finding and rigidity problems that can both be characterized as static problems associated with tensegrity structures, [10, 11], [12], [13], [14], [15]. Lightweight space controllable structures are the target applications for tensegrity structures. Hence, lacking a systematic way for their optimal design becomes more significant.

This work is motivated by structural optimization problems already addressed by several authors. Optimization of topology of structures has been studied for a long time, [16], [17]. Several approaches for numerical optimization are known [18–22], with recent approaches being free material modelling [23] and optimization of trusses [24, 25]. In order to accommodate specifics of tensegrity structures our formulation includes tensegrity existence conditions that parameterize prestressed equilibrium of the structure. Practical reasons require incorporating constraints that preserve structural integrity by preventing different modes of failure of its elements. In contrast to optimization of trusses starting from a fully populated grid in [25], the maximum set of allowed geometries of the structure is not predefined in our formulation, since nodal positions are actually design variables. This paper also concerns the influence of different material parameters on the optimal topology with the focus on class–2 tensegrity towers.

The paper is outlined as follows. In Section 2 the parameterization of structure equilibria and its static response are formulated. Then, optimization variables and constraints are identified and defined. In Section 3, the formulation of the optimization problem is given in a form of a nonlinear program, along with the Jacobian of the nonlinear constraints. The class–2 tensegrity tower example follows in Section 4. A discussion and conclusions are given in Section 5 and Section 6.

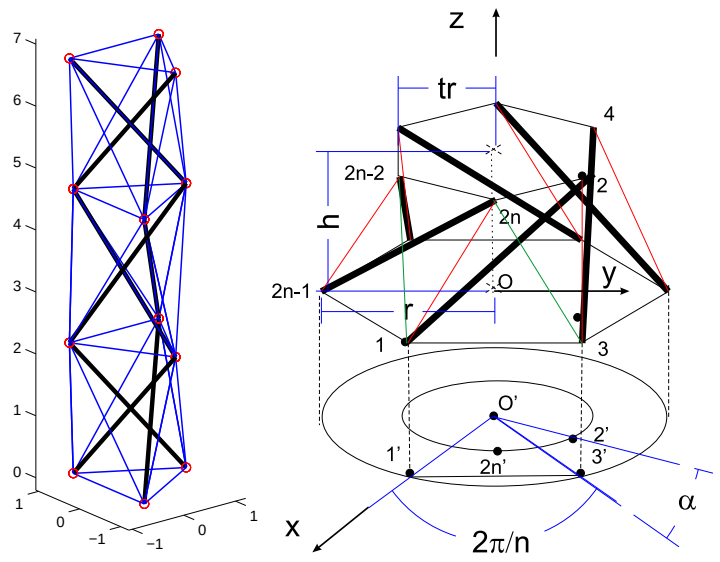

Figure 1. Class–2 tensegrity tower and geometry of its n–bar one–stage module

2. FORMULATION OF THE PROBLEM

The objective of this analysis is to design a class–two tensegrity tower that has for the given mass of the material available has the maximum stiffness. The total volume v_{total} can be used to fix the mass under the assumption that all elements are composed of the same material.

The tower depicted in Figure 1 represents a modular structure. For certain loading conditions, like for example symmetric compression or torsion with respect to the axis of symmetry of the tower, the stiffness of the overall structure can be modeled as a serial connection of the elastic substructures– the modules. Hence, the analysis of the related properties of the whole structure will be performed on its module whose geometry is depicted in Figure 1. The results obtained apply to tensegrity towers of arbitrary size as long as the loading conditions remain equivalent. The problem formulation will be given in a way that can accommodate a broader class of problems than the class–two tower module analysis. Specific that pertain to this particular example will be given in the context of the more general problem.

Let the set $\mathbb{N}$ of n_n nodes of a tensegrity structure be given, and let the node $\nu_j \in \mathbb{N}$ be located at the position defined by the nodal vector $\mathbf{p}_j \in \mathbb{R}^3$. Denote the set of all nodal vectors $\mathbb{P}$. Let the set $\mathbb{E}$ of n_e elements of the structure be given, and let $\mathbb{E}_s$ and $\mathbb{E}_b$ denote its partitions in the sets of n_s strings and n_b bars respectively. The scalar z_i in the definition of the element $e_i = \{[\nu_j, \nu_k], z_i\} \in \mathbb{E}$ that connects the nodes ν_j and ν_k of the tensegrity, identifies the type of the element so that,

$$z_i = \begin{cases} 1, & e_i \in \mathbb{E}_s, \\ -1, & e_i \in \mathbb{E}_b. \end{cases} \tag{1}$$

2.1. Tensegrity equilibrium

If the element vector $\mathbf{g}_i \in \mathbb{R}^3$ of the element $e_i = \{[\nu_j, \nu_k], z_i\}$ is defined as,

$$\mathbf{g}_i = \mathbf{p}_j - \mathbf{p}_k, \quad \|\mathbf{g}_i\|_2 = l_i,$$

then, the element force vector $\mathbf{f}_{ji} \in \mathbb{R}^3$ that represents the contribution of the internal force of the element e_i, to the balance of the forces at the node ν_j can be written as,

$$\mathbf{f}_{ji} = c_{ji}\lambda_i \mathbf{g}_i, \quad f_i = \lambda_i \|\mathbf{g}_i\| = \lambda_i l_i, \tag{2}$$

where element force coefficient λ_i is a scalar. Scalars c_{ji} in (2) that are defined as typical elements of the matrix $C(\mathbb{E}) \in \mathbb{R}^{n_n \times n_e}$, have one of the three possible values, $c_{ji} = \pm 1$ or $c_{ji} = 0$.

Let $\mathbb{R}^n_m$ denote the vector space of vectors $\mathbf{x}$ that have the following structure:

$$\mathbf{x} \in \mathbb{R}^n_m \Rightarrow \mathbf{x}^T = \left[\begin{array}{cccc} \mathbf{x}_1^T & \mathbf{x}_2^T & \dots & \mathbf{x}_n^T \end{array} \right], \quad \mathbf{x}_i \in \mathbb{R}^m, \quad \mathbb{R}^m = \mathbb{R}^m_1 \tag{3}$$

Vector of nodal vectors $\mathbf{p} \in \mathbb{R}^{n_n}_3$, vector of element vectors $\mathbf{g}(\mathbb{E}, \mathbf{p}) \in \mathbb{R}^{n_e}_3$, vector of force coefficients $\boldsymbol{\lambda} \in \mathbb{R}^{n_e}$ and vector $\mathbf{z} \in \mathbb{R}^{n_e}$ are formed by collecting all node vectors $\mathbf{p}_i$, element vectors $\mathbf{g}_i$, force coefficients λ_i and all individual element type identifiers,

$$\mathbf{p} = \left[\begin{array}{c} \mathbf{p}_1 \\ \mathbf{p}_2 \\ \vdots \\ \mathbf{p}_{n_n} \end{array} \right], \ \mathbf{g} = \left[\begin{array}{c} \mathbf{g}_1 \\ \mathbf{g}_2 \\ \vdots \\ \mathbf{g}_{n_e} \end{array} \right], \ \boldsymbol{\lambda} = \left[\begin{array}{c} \lambda_1 \\ \lambda_2 \\ \vdots \\ \lambda_{n_e} \end{array} \right], \ \mathbf{z} = \left[\begin{array}{c} z_1 \\ z_2 \\ \vdots \\ z_{n_e} \end{array} \right].$$

Define the linear operator $\tilde{\cdot}$ acting on the vector $\mathbf{x} \in \mathbb{R}^n_m$ is defined as follows,

$$\tilde{\mathbf{x}} := blockdiag\{\mathbf{x}_1, \dots, \mathbf{x}_i, \dots, \mathbf{x}_n\} \in \mathbb{R}^{mn \times n}, \quad \mathbf{x}_i \in \mathbb{R}^m.$$

Define the linear operator $\hat{(\cdot)}$ acting on the vector $\mathbf{x} \in \mathbb{R}^n$ by,

$$\hat{\mathbf{x}} := \tilde{\mathbf{x}} \otimes I_3 \in \mathbb{R}^{3n \times 3n}. \tag{4}$$

Let the member-node incidence matrix of the oriented graph associated with $\mathbb{E}$ be denoted $M(\mathbb{E}) \in \mathbb{R}^{n_e \times n_n}$ and let $\mathbf{M} \in \mathbb{R}^{3n_e \times 3n_n}$ be defined as $\mathbf{M} = M \otimes I_3$. The typical element m_{ij} of the matrix M is $m_{ij} = 1$ or $m_{ij} - 1$ if the element e_i terminates at or emanates from the node ν_j, otherwise $m_{ij} = 0$. Let the n_s string elements in $\mathbb{E}_s$ be numbered first. Then, vector $\mathbf{g}$ and matrix $\mathbf{M}$ are related and partitioned as follows,

$$\mathbf{g}(\mathbf{p}) = \left[\begin{array}{c} \mathbf{g}_s(\mathbf{p}) \\ \mathbf{g}_b(\mathbf{p}) \end{array} \right] = \mathbf{M}\mathbf{p}, \quad \mathbf{M} = \left[\begin{array}{c} \mathbf{S}^T \\ \mathbf{B}^T \end{array} \right], \quad \mathbf{S} \in \mathbf{R}^{3n_n \times 3n_s}.$$

One can show that matrices $\mathbf{M}(\mathbb{E})$ and $\mathbf{C}(\mathbb{E}) = C(\mathbb{E}) \otimes I_3$ are related as follows,

$$\mathbf{M} = \left[\begin{array}{c} \mathbf{S}^T \\ \mathbf{B}^T \end{array} \right], \quad \mathbf{C} = \left[\begin{array}{cc} -\mathbf{S} & \mathbf{B} \end{array} \right]. \tag{5}$$

Throughout the text it will be assumed that the string elements of the tensegrity structure are numbered first so that the vectors $(\cdot) \in \mathbb{R}^{n_e}_m$ of all different properties associated with the elements of the structure can be partitioned as,

$$(\cdot)(\mathbf{p}) = \left[\begin{array}{c} (\cdot)_s(\mathbf{p}) \\ (\cdot)_b(\mathbf{p}) \end{array} \right], \quad (\cdot)_s \in \mathbb{R}^{n_s}_m, \quad (\cdot) \in \mathbb{R}^{n_b}_m. \tag{6}$$

Let the vectors $\mathbf{f}^e_j(\mathbf{p}) \in \mathbb{R}^3$ and $\mathbf{f}^e_j(\mathbf{p}) \in \mathbb{R}^3$ represent respectively the collection of all the external force vectors and constraint forces acting at the node ν_j in the given configuration $\mathbf{p}$,

$$\mathbf{f}^e = \left[\begin{array}{c} \mathbf{f}^e_1 \\ \mathbf{f}^e_2 \\ \vdots \\ \mathbf{f}^e_{n_n} \end{array} \right], \quad \mathbf{f}^c = \left[\begin{array}{c} \mathbf{f}^c_1 \\ \mathbf{f}^c_2 \\ \vdots \\ \mathbf{f}^c_{n_n} \end{array} \right]. \tag{7}$$

Then, the equilibrium conditions for the structure with properly loaded strings in the configuration $\mathbf{p}$ can be written as,

$$\mathbf{C}\hat{\boldsymbol{\lambda}}(\mathbf{p})\mathbf{M}\mathbf{p} + \mathbf{f}^e(\mathbf{p}) + \mathbf{f}^c(\mathbf{p}) = 0, \tag{8}$$

$$\lambda_i(\mathbf{p}) \geq 0, \quad e_i \in \mathbb{E}_s. \tag{9}$$

2.1.1. Linear elastic material model

The relationship between the force coefficient variables $\boldsymbol{\lambda}(\mathbf{p})$ and actual structure parameters depends on the strain–stress relationship for the material used to build elastic elements of the structure. The force coefficients $\boldsymbol{\lambda}(\mathbf{p})$ at any equilibrium configuration $\mathbf{p}$ can be computed from Hooke's law for linear elastic materials. Define volumes v_i, rest lengths l_{0_i} and Young's modulus y_i, of cylindrical elements and collect them in the corresponding vectors $\mathbf{l}_0 \in \mathbb{R}^{n_e}$, $\mathbf{v} \in \mathbb{R}^{n_e}$ and $\mathbf{y} \in \mathbb{R}^{n_e}$,

$$\mathbf{l}_0 = \begin{bmatrix} l_{0_1} \\ l_{0_2} \\ \vdots \\ l_{0_{n_e}} \end{bmatrix} = \begin{bmatrix} \mathbf{l}_{0_s} \\ \mathbf{l}_{0_b} \end{bmatrix}, \quad \mathbf{v} = \begin{bmatrix} v_1 \\ v_2 \\ \vdots \\ v_{n_e} \end{bmatrix} = \begin{bmatrix} \mathbf{v}_s \\ \mathbf{v}_b \end{bmatrix}, \quad y = \begin{bmatrix} y_1 \\ y_2 \\ \vdots \\ y_{n_n} \end{bmatrix} = \begin{bmatrix} \mathbf{y}_s \\ \mathbf{y}_b \end{bmatrix}.$$

Then the force coefficients can be computed as,

$$\lambda_i(\mathbf{p}) = \frac{\mathbf{f}_i(\mathbf{p})}{l_i(\mathbf{p})} = z_i \frac{y_i v_i}{l_i(\mathbf{p}) l_{0_i}^2}(l_i(\mathbf{p}) - l_{0_i}), \tag{10}$$

so that (9) can be rewritten in the equivalent form,

$$-(l_i(\mathbf{p}) - l_{0_i}) \leq 0, \quad e_i \in \mathbb{E}_s. \tag{11}$$

2.2. Equilibrium conditions in absence of external forces

The equilibrium condition in (8), with no external load, $\mathbf{f}^e(\mathbf{p}) = 0$, becomes

$$\mathbf{C}\hat{\boldsymbol{\lambda}}(\mathbf{p})\mathbf{M}\mathbf{p} + \mathbf{f}^c(\mathbf{p}) = 0, \tag{12}$$

$$-(l_i(\mathbf{p}) - l_{0_i}) \leq 0 \quad e_i \in \mathbb{E}_s, \tag{13}$$

where $\boldsymbol{\lambda}(\mathbf{p})$ is given by (10).

2.3. Large displacement static response - loaded equilibrium conditions

Once the external force $\mathbf{f}^e$ is applied upon the structure in equilibrium configuration $\mathbf{p}$, it deformes to a new equilibrium configuration, $\mathbf{p} + \mathbf{u}$. The vector of nodal displacements $\mathbf{u} \in \mathbb{R}_3^{n_n}$,

$$\mathbf{u}^T = \begin{bmatrix} \mathbf{u}_1^T & \mathbf{u}_2^T & \dots & \mathbf{u}_{n_n}^T \end{bmatrix},$$

can be computed without any assumptions on the size of the displacement $\mathbf{u}_j \in \mathbb{R}^3$ of the node ν_j. Equation (10) defines the equilibrium force coefficient vector $\boldsymbol{\lambda}(\mathbf{p} + \mathbf{u})$ in any equilibrium configuration $\mathbf{p} + \mathbf{u}$ and this relationship holds true independently on the magnitude of $\mathbf{u}$. Hence, nodal displacements $\mathbf{u}$ of the loaded structure can be computed directly from the structure equilibrium conditions in the configuration $\mathbf{p} + \mathbf{u}$, instead of the linearization method that involves the computation of the structure stiffness matrix. From (8), substituting (9) with (11), equilibrium conditions for the configuration $\mathbf{p} + \mathbf{u}$ become,

$$\mathbf{C}\hat{\boldsymbol{\lambda}}(\mathbf{p} + \mathbf{u})\mathbf{M}(\mathbf{p} + \mathbf{u}) + \mathbf{f}^e(\mathbf{p} + \mathbf{u}) + \mathbf{f}^c(\mathbf{p} + \mathbf{u}) = 0, \tag{14}$$

$$-(l_i(\mathbf{p} + \mathbf{u}) - l_{0_i}) \leq 0 \quad e_i \in \mathbb{E}_s, \tag{15}$$

where $\boldsymbol{\lambda}(\mathbf{p} + \mathbf{u})$ is given by (10). The constraint in (15) guaranties that the string elements are not compressed in this new equilibrium.

The relationship between the nodal displacements $\mathbf{u}$ and the external forces $\mathbf{f}^e$ in (14) is nonlinear although the elements of the structure are linear elastic. The nonlinear structure model in (14) parameterizes all equilibrium configurations of the structure under the external force $\mathbf{f}^e$, regardless of them being unique. It can be seen that the non-uniqueness of the equilibrium geometry, $\mathbf{p} + \mathbf{u}$ resulting from global buckling or other nonlinear effects is also accommodated by this model.

2.4. Defining the optimization objective and identifying the tensegrity structure parameters

2.4.1. Optimization objectives

One can define different criteria to measure structure stiffness. The work done by the external forces, $\mathbf{f}^e$, to deform the structure from configuration $\mathbf{p}$ to $\mathbf{p}+\mathbf{u}$, is one possible measure. The inner product, $\frac{1}{2}\mathbf{f}^{eT}\mathbf{u}$, is an approximation of the work done and will be called approximate compliance since it is computed from the nonlinear structure model (14). Computed values of the approximate compliance, $\frac{1}{2}\mathbf{f}^{eT}\mathbf{u}$, are generally lower than the compliance, $\frac{1}{2}\mathbf{f}^{eT}\mathbf{u}^l$, if the nodal displacements, $\mathbf{u}^l$, were computed from the linearized structure model. This is due to the nonlinear stiffening effect.

If the approximate compliance is the measure of the stiffness, only the nodal displacements of the nodes at which the external forces act are penalized. An elliptical norm $\mathbf{u}^T Q\mathbf{u},\ Q \succeq 0$ can be used as the stiffness measure to penalize other nodal displacements.

2.4.2. Design variables

From (8)-(9), (14)-(15) and (10) it is clear that for the tensegrity structure with connectivity $\mathbb{E}$ the parameters that define its static response $\mathbf{u}$ are the nodal vector $\mathbf{p}$, element rest lengths $\mathbf{l}_0 \in \mathbb{R}^{n_e}$, and element volumes $\mathbf{v} \in \mathbb{R}^{n_e}$. These three structure parameters will be variables in the optimization problem. The domains of their feasible values are $\mathbf{l}_0 > 0$ and $\mathbf{v} \geq 0$. Note that the presence of the element e_i in the set $\mathbb{E}$ defines allowable element connections in the structure, but that the volume $v_i > 0$ is the actual indicator of the presence of the element in the structure. For the structure comprised of the elements built of the same material, the constraint that fixes its total mass can be written as $\sum v_i = v_{total}$.

2.4.3. Symmetry treatment

The domain of the variables in the problem has to be reduced to account for the symmetry requirements in the design. With the structure parameters identified so far, there can be associated two classes of symmetry. The first symmetry is the nodal symmetry. It can be shown that the nodal symmetry constraint can be cast in the following linear form,

$$\mathbf{p} = \mathcal{R}\underline{\mathbf{p}}, \tag{16}$$

where the matrix $\mathcal{R}$ depends on the particular nodal symmetry and is defined in [14]. Obviously, the nodal symmetry constraint represents a reduction in the number of independent geometry variables from $\mathbf{p} \in \mathbb{R}_3^{n_n}$ to $\underline{\mathbf{p}} \in \mathbb{R}_3^{n_c}$, where the vector $\underline{\mathbf{p}}$ is the nodal vector of the subset of nodes $\underline{\mathbb{N}} \in \mathbb{N}$. The second symmetry is the symmetry of the sets of parameters $\mathbf{l_0}$ and $\mathbf{v}$ associated with the elements of the structure. It can also be regarded as a reduction of the number of variables and cast in the linear form,

$$\mathbf{l_0} = E\underline{\mathbf{l_0}}, \quad \mathbf{v} = E\underline{\mathbf{v}}, \quad E \in \mathbb{R}^{n_e \times \underline{n}_e}, \quad \underline{\mathbf{l}}_0, \underline{\mathbf{v}} \in \mathbb{R}^{\underline{n}_e}, \tag{17}$$

where the sparse matrix E relates the vector of different typical elements with the full vector of the variables. It is possible to define and impose other symmetries of the structure. Symmetry of the external force and nodal displacements are two examples. These additional symmetries will not be exploited in the problem formulation because they are not independent from each other, and if not defined consistently with other constraints they can render an infeasible problem.

2.5. Shape constraints and boundary conditions

2.5.1. Shape constraints

A desired shape of the structure before external forces $\mathbf{f}^e$ have been applied on it, can be specified by defining the form of the general shape constraint $\boldsymbol{\varphi}(\underline{\mathbf{p}}) = 0$. To ensure that the tensegrity structure can be supported at the desired locations and that the external load acting at specified locations can be attached to it, the tensegrity structure in the configuration $\mathbf{p} = \mathcal{R}\underline{\mathbf{p}}$ has to satisfy the shape constraints in the linear form,

$$\mathbf{P}\underline{\mathbf{p}} = \underline{\mathbf{p}}^c, \tag{18}$$

where $\mathbf{P}$ and $\underline{\mathbf{p}}^c$ are a given matrix and vector.

The element length constraint also belongs to the category of geometry constraints.

$$l_i(\mathbf{p}) > l_{min_i}, \quad l_i(\mathbf{p}+\mathbf{u}) > l_{min_i} \tag{19}$$

One of the reasons for constraining the minimal length of the elements is the limited ability to manufacture structures with elements that are too short. This constraint also guarantees that the Jacobian of the constraints is well defined since it involves inverses of element lengths.

2.5.2. Boundary conditions treatment

The only constraint on structure displacements $\mathbf{u}$ that will be considered here is the consequence of attaching the nodes of the structure to linear supports. In that case, the admissible nodal displacements must satisfy the following linear constraint,

$$C_u\mathbf{u} = 0, \tag{20}$$

where the structure of the constraint matrix $C_u \in \mathbb{R}^{n_c \times 3n_n}$ depends on the type of the supports that structure is attached to. It can be shown that the constraint forces, $\mathbf{f}^c(\mathbf{p})$, in any configuration $\mathbf{p}$, are the vectors in the left range space of the matrix C_u. Hence, $\mathbf{f}^c(\mathbf{p})$ can be written as,

$$\mathbf{f}^c(\mathbf{p}) = C_u^T\boldsymbol{\lambda}^c(\mathbf{p}), \tag{21}$$

for some choice of the Lagrange multipliers $\boldsymbol{\lambda}^c \in \mathbb{R}^{n_c}$. Assume that only n_c independent boundary conditions are defined so that matrix C_u has a full row rank. Let the singular value decomposition of the matrix C_u be given as,

$$C_u = U\Sigma V^T = U\begin{bmatrix} \Sigma_1 & 0 \end{bmatrix}\begin{bmatrix} V_1^T \\ V_2^T \end{bmatrix} = U\Sigma_1 V_1^T, \quad C_u^T = V_1\Sigma_1 U^T$$
$$UU^T = U^TU = I, \quad VV^T = V^TV = I.$$

An equivalent formulation of the equilibrium conditions in (14) and (8) can be obtained by using (21) in these equations and multiplying them from the left with the orthonormal full rank matrix V^T yielding

$$\begin{bmatrix} V_1^T \\ V_2^T \end{bmatrix}(\mathbf{C}\hat{\boldsymbol{\lambda}}(\mathbf{p})\mathbf{M}(\mathbf{p}) + \mathbf{f}^e(\mathbf{p})) + \begin{bmatrix} \Sigma_1 U^T \\ 0 \end{bmatrix}\boldsymbol{\lambda}^c(\mathbf{p}) = 0. \tag{22}$$

It is clear from (22) that the solution of the problem can be split into two parts. Lagrange multipliers $\boldsymbol{\lambda}^c$ do not appear as the variable in the first set of equations,

$$V_2^T(\mathbf{C}\hat{\boldsymbol{\lambda}}(\mathbf{p})\mathbf{M}(\mathbf{p}) + \mathbf{f}^e(\mathbf{p})) = 0, \tag{23}$$

whereas the second set of equations,

$$V_1^T(\mathbf{C}\hat{\boldsymbol{\lambda}}(\mathbf{p})\mathbf{M}(\mathbf{p}) + \mathbf{f}^e(\mathbf{p})) + \Sigma_1 U^T\boldsymbol{\lambda}^c(\mathbf{p}) = 0, \tag{24}$$

gives the solution for the Lagrange multipliers $\boldsymbol{\lambda}^c$ and the constraint forces $\mathbf{f}^c$,

$$\boldsymbol{\lambda}^c(\mathbf{p}) = -U\Sigma_1^{-1}V_1^T(\mathbf{C}\hat{\boldsymbol{\lambda}}(\mathbf{p})\mathbf{M}(\mathbf{p}) + \mathbf{f}^e(\mathbf{p})),$$
$$\mathbf{f}^c(\mathbf{p}) = C_u^T\boldsymbol{\lambda}^c(\mathbf{p}) = -C_u^TU\Sigma_1^{-1}V_1^T(\mathbf{C}\hat{\boldsymbol{\lambda}}(\mathbf{p})\mathbf{M}(\mathbf{p}) + \mathbf{f}^e(\mathbf{p})).$$

2.6. Strength constraints

All elements of a tensegrity structure must be constrained from yielding in order to preserve structure integrity in both unloaded configuration $\mathbf{p}$ and loaded configuration $\mathbf{p}+\mathbf{u}$. These constraints can be defined from the Hooke's law for the axially loaded elements as,

$$\epsilon_i(\mathbf{p})y_i = z_i\frac{l_i(\mathbf{p}) - l_{0_i}}{l_{0_i}}y_i \le \sigma_i,$$
$$\epsilon_i(\mathbf{p}+\mathbf{u})y_i = z_i\frac{l_i(\mathbf{p}+\mathbf{u}) - l_{0_i}}{l_{0_i}}y_i \le \sigma_i,$$

where σ_i is the yield stress of the element e_i. An equivalent form of these constraints is,

$$z_i(l_i(\mathbf{p}) - l_{0_i})y_i - \sigma_i l_{0_i} \leq 0,$$
$$z_i(l_i(\mathbf{p}+\mathbf{u}) - l_{0_i})y_i - \sigma_i l_{0_i} \leq 0.$$

Since bar elements are allowed to be under tension, additional constraints must be defined to account for this fact,

$$y_i(l_i(\mathbf{p}) - l_{0_i}) - l_{0_i}\sigma \leq 0, \quad e_i \in \mathbb{E}_b, \tag{25}$$
$$y_i(l_i(\mathbf{p}+\mathbf{u}) - l_{0_i}) - l_{0_i}\sigma \leq 0, \quad e_i \in \mathbb{E}_b. \tag{26}$$

2.7. Buckling constraints

Since bar elements are the only elements that may be compressed, a buckling constraint is applied only to bars. The maximum magnitude, f_{max_i}, of the compressive force, f_i, that the bars can be loaded with, is defined by Euler's formula,

$$f_i \leq f_{max_i} = \frac{\pi^2 y_i I_{min_i}}{l_{0_i}^2}, \tag{27}$$

where I_{min_i} is the minimal moment of inertia of the cross section of the element. Assuming that all bars have a round cross section with radius r_i, $I_{i_{min}}$ is defined as,

$$I_{min_i} = \frac{\pi r_i^4}{4}.$$

Then, using

$$r_i^2 = \frac{v_i}{\pi l_{0_i}},$$

$I_{i_{min}}$ can be computed as,

$$I_{i_{min}} = \frac{v_i^2}{4\pi l_{0_i}^2}. \tag{28}$$

From (2),(10) and (28) after manipulating (27), the bar buckling constraint can be rewritten as,

$$-l_0^2(l_i(\mathbf{p}) - l_{0_i}) - \frac{\pi}{4}v_i \leq 0, \quad e_i \in \mathbb{E}_b.$$

The buckling constraint must be satisfied in both unloaded configuration $\mathbf{p}$ and loaded configuration $\mathbf{p}+\mathbf{u}$, so that it is finally written as,

$$-l_0^2(l_i(\mathbf{p}) - l_{0_i}) - \frac{\pi}{4}v_i \leq 0, \quad e_i \in \mathbb{E}_b, \tag{29}$$
$$-l_0^2(l_i(\mathbf{p}+\mathbf{u}) - l_{0_i}) - \frac{\pi}{4}v_i \leq 0, \quad e_i \in \mathbb{E}_b. \tag{30}$$

3. NONLINEAR PROGRAM FORMULATION

Keeping strength and buckling constraint in the problem for zero volume elements may produce conservative results. Hence, these constraints for a zero volume element e_i should be relaxed by multiplying them with the element volume v_i. The optimal mass–to–stiffness ratio optimization problem for the tensegrity structure of the connectivity $\mathbb{E}$, made of the material $\{y, \sigma\}$, loaded with external force $\mathbf{f}^e$, and defined shape and displacement

constraints is written as,

$$
\begin{aligned}
&\text{Given data} && \mathbf{C}(\mathbb{E}), \mathbf{M}(\mathbb{E}), \mathbf{z}, \mathbf{y}, \mathbf{f}^e, \mathbf{C}_u, V_2, \mathbf{P}, \underline{\mathbf{p}}^c, \mathcal{R}, E, \sigma, v_{total}, \mathbf{l}_{0min}, \mathbf{l}_{min}, \bar{\mathbf{l}}_{min} \\
&\min_{\underline{\mathbf{p}}, \underline{\mathbf{l}}_0, \underline{\mathbf{v}}, \mathbf{u}} && \mathbf{f}^{eT}\mathbf{u} \\
&\text{subject to} && \\
&\text{linear constraints :} && \mathbf{P}\underline{\mathbf{p}} = \underline{\mathbf{p}}^c, \\
& && -\underline{\mathbf{l}}_0 + \mathbf{l}_{0min} \leq 0, \\
& && -\underline{\mathbf{v}} \leq 0, \\
& && \begin{bmatrix} 1 & 1 & 1 & . & 1 \end{bmatrix} \mathbf{v} - v_{total} = 0, \\
& && \mathbf{C}_u \mathbf{u} = 0, \\
&\text{nonlinear constraints :} && \boldsymbol{\varphi}(\underline{\mathbf{p}}) = 0, \\
& && V_2^T \mathbf{C} \hat{\boldsymbol{\lambda}}(\mathbf{p}) \mathbf{M} \mathbf{p} = 0, \\
& && V_2^T \mathbf{C} \hat{\boldsymbol{\lambda}}(\mathbf{p}+\mathbf{u}) \mathbf{M}(\mathbf{p}+\mathbf{u}) + V_2^T \mathbf{f}^e = 0, \\
& && -\tilde{\mathbf{v}}_s(\mathbf{l}_s(\mathbf{p}) - \mathbf{l}_{0s}) \leq 0, \\
& && -\tilde{\mathbf{v}}_s(\mathbf{l}_s(\mathbf{p}+\mathbf{u}) - \mathbf{l}_{0s}) \leq 0, \\
& && -\mathbf{l}(\mathbf{p}) + \mathbf{l}_{min} \leq 0, \\
& && -\mathbf{l}(\mathbf{p}+\mathbf{u}) + \bar{\mathbf{l}}_{min} \leq 0, \\
& && \tilde{\mathbf{v}}(\tilde{\mathbf{z}}\tilde{\mathbf{y}}(\mathbf{l}(\mathbf{p}) - \mathbf{l}_0) - \tilde{\boldsymbol{\sigma}}\mathbf{l}_0) \leq 0, \\
& && \tilde{\mathbf{v}}_b(\tilde{\mathbf{y}}_b(\mathbf{l}_b(\mathbf{p}) - \mathbf{l}_{0_b}) - \tilde{\boldsymbol{\sigma}}_b\mathbf{l}_{0_b}) \leq 0, \\
& && \tilde{\mathbf{v}}(\tilde{\mathbf{z}}\tilde{\mathbf{y}}(\mathbf{l}(\mathbf{p}+\mathbf{u}) - \mathbf{l}_0) - \tilde{\boldsymbol{\sigma}}\mathbf{l}_0) \leq 0, \\
& && \tilde{\mathbf{v}}_b(\tilde{\mathbf{y}}_b(\mathbf{l}_b(\mathbf{p}+\mathbf{u}) - \mathbf{l}_{0_b}) - \tilde{\boldsymbol{\sigma}}_b\mathbf{l}_{0_b}) \leq 0, \\
& && -\tilde{\mathbf{v}}_b(\tilde{\mathbf{l}}_{0_b}^2(\mathbf{l}_b(\mathbf{p}) - \mathbf{l}_{0_b}) - \frac{\pi}{4}\mathbf{v}_b) \leq 0, \\
& && -\tilde{\mathbf{v}}_b(\tilde{\mathbf{l}}_{0_b}^2(\mathbf{l}_b(\mathbf{p}+\mathbf{u}) - \mathbf{l}_{0_b}) - \frac{\pi}{4}\mathbf{v}_b) \leq 0, \\
&\text{where :} && \mathbf{p} = \mathcal{R}\underline{\mathbf{p}}, \quad l_i(\mathbf{p}) = \|\mathbf{g}_i(\mathbf{p})\|_2, \quad \mathbf{g}(\mathbf{p}) = \mathbf{M}\mathbf{p}, \\
& && \mathbf{l}_0 = E\underline{\mathbf{l}}_0, \quad \mathbf{v} = E\underline{\mathbf{v}}, \\
& && \lambda_i(\mathbf{p}) = \frac{z_i y_i v_i}{l_i(\mathbf{p}) l_{0_i}^2}(l_i(\mathbf{p}) - l_{0_i}).
\end{aligned}
$$

3.1. Jacobian of the nonlinear constraints

The jacobian of the nonlinear constraints is given in the following matrix,where the operator $\bar{x}$ denotes $\bar{x} = x(\mathbf{p}+\mathbf{u})$.

$$
J = \begin{bmatrix}
\delta\boldsymbol{\varphi}(\underline{\mathbf{p}})/\delta\underline{\mathbf{p}} & 0 & 0 & 0 \\
V_2^T\mathbf{C}\hat{\boldsymbol{\lambda}}\mathbf{M} - V_2^T\mathbf{C}\tilde{\mathbf{g}}\tilde{\mathbf{y}}\tilde{\mathbf{v}}\tilde{\mathbf{l}}_0^{-1}\tilde{\mathbf{l}}^{-3}\tilde{\mathbf{g}}^T\mathbf{C}^T & V_2^T\mathbf{C}\tilde{\mathbf{g}}\tilde{\mathbf{z}}\tilde{\mathbf{y}}\tilde{\mathbf{v}}(-2\tilde{\mathbf{l}}_0^{-3} + \tilde{\mathbf{l}}_0^{-2}\tilde{\mathbf{l}}^{-1}) & V_2^T\mathbf{C}\tilde{\mathbf{g}}\tilde{\mathbf{z}}\tilde{\mathbf{y}}\tilde{\mathbf{l}}_0^{-2}\tilde{\mathbf{l}}^{-1}(\tilde{\mathbf{l}} - \tilde{\mathbf{l}}_0) & 0 \\
V_2^T\mathbf{C}\hat{\bar{\boldsymbol{\lambda}}}\mathbf{M} - V_2^T C\tilde{\bar{\mathbf{g}}}\tilde{\bar{\mathbf{y}}}\tilde{\bar{\mathbf{v}}}\tilde{\bar{\mathbf{l}}}_0^{-1}\tilde{\bar{\mathbf{l}}}^{-3}\tilde{\bar{\mathbf{g}}}^T\mathbf{C}^T & V_2^T\mathbf{C}\tilde{\bar{\mathbf{g}}}\tilde{\bar{\mathbf{z}}}\tilde{\bar{\mathbf{y}}}\tilde{\bar{\mathbf{v}}}(-2\tilde{\bar{\mathbf{l}}}_0^{-3} + \tilde{\bar{\mathbf{l}}}_0^{-2}\tilde{\bar{\mathbf{l}}}^{-1}) & V_2^T\mathbf{C}\tilde{\bar{\mathbf{g}}}\tilde{\bar{\mathbf{z}}}\tilde{\bar{\mathbf{y}}}\tilde{\bar{\mathbf{l}}}_0^{-2}\tilde{\bar{\mathbf{l}}}^{-1}(\tilde{\bar{\mathbf{l}}} - \tilde{\bar{\mathbf{l}}}_0) & V_2^T\mathbf{C}\hat{\bar{\boldsymbol{\lambda}}}\mathbf{M} - V_2^T C\tilde{\bar{\mathbf{g}}}\tilde{\bar{\mathbf{y}}}\tilde{\bar{\mathbf{v}}}\tilde{\bar{\mathbf{l}}}_0^{-1}\tilde{\bar{\mathbf{l}}}^{-3}\tilde{\bar{\mathbf{g}}}^T\mathbf{C}^T \\
\tilde{\mathbf{v}}_s\tilde{\mathbf{l}}_s^{-1}\tilde{\mathbf{g}}_s^T\mathbf{S}^T & \tilde{\mathbf{v}}_s & -(\tilde{\mathbf{l}}_s - \tilde{\mathbf{l}}_{0_s}) & 0 \\
\tilde{\mathbf{v}}_s\tilde{\bar{\mathbf{l}}}_s^{-1}\tilde{\bar{\mathbf{g}}}_s^T\mathbf{S}^T & \tilde{\mathbf{v}}_s & -(\tilde{\bar{\mathbf{l}}}_s - \tilde{\bar{\mathbf{l}}}_{0_s}) & \tilde{\mathbf{v}}_s\tilde{\bar{\mathbf{l}}}_s^{-1}\tilde{\bar{\mathbf{g}}}_s^T\mathbf{S}^T \\
-\tilde{\mathbf{l}}^{-1}\tilde{\mathbf{g}}^T\mathbf{M} & 0 & 0 & 0 \\
-\tilde{\bar{\mathbf{l}}}^{-1}\tilde{\bar{\mathbf{g}}}^T\mathbf{M} & 0 & 0 & -\tilde{\bar{\mathbf{l}}}^{-1}\tilde{\bar{\mathbf{g}}}^T\mathbf{M} \\
\tilde{\mathbf{z}}\tilde{\mathbf{v}}\tilde{\mathbf{y}}\tilde{\mathbf{l}}^{-1}\tilde{\mathbf{g}}^T\mathbf{M} & -\tilde{\mathbf{z}}\tilde{\mathbf{y}}\tilde{\mathbf{v}} - \tilde{\boldsymbol{\sigma}}\tilde{\mathbf{v}} & \tilde{\mathbf{z}}\tilde{\mathbf{y}}(\tilde{\mathbf{l}} - \tilde{\mathbf{l}}_0) - \tilde{\mathbf{l}}_0\tilde{\boldsymbol{\sigma}} & 0 \\
\tilde{\mathbf{v}}_b\tilde{\mathbf{y}}_b\tilde{\mathbf{l}}_b^{-1}\tilde{\mathbf{g}}_b^T\mathbf{B}^T & \tilde{\mathbf{y}}_b\tilde{\mathbf{v}}_b - \tilde{\boldsymbol{\sigma}}_b\tilde{\mathbf{v}}_b & \tilde{\mathbf{y}}_b(\tilde{\mathbf{l}}_b - \tilde{\mathbf{l}}_{0_b}) - \tilde{\mathbf{l}}_{0_b}\tilde{\boldsymbol{\sigma}}_b & 0 \\
\tilde{\mathbf{z}}\tilde{\mathbf{v}}\tilde{\mathbf{y}}\tilde{\bar{\mathbf{l}}}^{-1}\tilde{\bar{\mathbf{g}}}^T\mathbf{M} & -\tilde{\mathbf{z}}\tilde{\mathbf{y}}\tilde{\mathbf{v}} - \tilde{\boldsymbol{\sigma}}\tilde{\mathbf{v}} & \tilde{\mathbf{z}}\tilde{\mathbf{y}}(\tilde{\bar{\mathbf{l}}} - \tilde{\bar{\mathbf{l}}}_0) - \tilde{\bar{\mathbf{l}}}_0\tilde{\boldsymbol{\sigma}} & \tilde{\mathbf{z}}\tilde{\mathbf{v}}\tilde{\mathbf{y}}\tilde{\bar{\mathbf{l}}}^{-1}\tilde{\bar{\mathbf{g}}}^T\mathbf{M} \\
\tilde{\mathbf{v}}_b\tilde{\mathbf{y}}_b\tilde{\bar{\mathbf{l}}}_b^{-1}\tilde{\bar{\mathbf{g}}}_b^T\mathbf{B}^T & \tilde{\mathbf{y}}_b\tilde{\mathbf{v}}_b - \tilde{\boldsymbol{\sigma}}_b\tilde{\mathbf{v}}_b & \tilde{\mathbf{y}}_b(\tilde{\bar{\mathbf{l}}}_b - \tilde{\bar{\mathbf{l}}}_{0_b}) - \tilde{\bar{\mathbf{l}}}_{0_b}\tilde{\boldsymbol{\sigma}}_b & \tilde{\mathbf{v}}_b\tilde{\mathbf{y}}_b\tilde{\bar{\mathbf{l}}}_b^{-1}\tilde{\bar{\mathbf{g}}}_b^T\mathbf{B}^T \\
-\tilde{\mathbf{v}}_b\tilde{\mathbf{l}}_{0_b}^2\tilde{\mathbf{l}}_b^{-1}\tilde{\mathbf{g}}_b^T\mathbf{B}^T & (3\tilde{\mathbf{l}}_{0_b}^2 - 2\tilde{\mathbf{l}}_{0_b}\tilde{\mathbf{l}}_b)\tilde{\mathbf{v}}_b & -\tilde{\mathbf{l}}_{0_b}^2(\tilde{\mathbf{l}}_b - \tilde{\mathbf{l}}_{0_b}) - \frac{\pi}{2}\tilde{\mathbf{v}}_b & 0 \\
-\tilde{\mathbf{v}}_b\tilde{\mathbf{l}}_{0_b}^2\tilde{\bar{\mathbf{l}}}_b^{-1}\tilde{\bar{\mathbf{g}}}_b^T\mathbf{B}^T & (3\tilde{\mathbf{l}}_{0_b}^2 - 2\tilde{\mathbf{l}}_{0_b}\tilde{\bar{\mathbf{l}}}_b)\tilde{\mathbf{v}}_b & -\tilde{\mathbf{l}}_{0_b}^2(\tilde{\bar{\mathbf{l}}}_b - \tilde{\mathbf{l}}_{0_b}) - \frac{\pi}{2}\tilde{\mathbf{v}}_b & -\tilde{\mathbf{v}}_b\tilde{\mathbf{l}}_{0_b}^2\tilde{\bar{\mathbf{l}}}_b^{-1}\tilde{\bar{\mathbf{g}}}_b^T\mathbf{B}^T
\end{bmatrix}
$$

4. OPTIMIZATION OF THE TOWER MODULE

The solutions for the problems given here are obtained using the SNOPT 6.1 [26] software package for sparse nonlinear optimization. The package uses the sequential quadratic programming (SQP) method. All constraint Jacobians and objective gradients were made available during the execution of the code in its sparse mode.

4.1. Compressive load case

We investigate the optimal topology of the three–bar module under a unit vertical compressive load applied to each of the top nodes of the module. The formulation of the constraints in the module optimization must accommodate structure symmetry, support conditions, and position of the nodes at which the load is applied. Due to the module symmetry, only the positions of the nodes at $\mathbf{p}_1$ and $\mathbf{p}_2$ serve as the variables in the problem. The position of the node at $\mathbf{p}_2$ is eliminated as the variable in order to guarantee that the external load can be attached to the structure at the desired location $\mathbf{p}_2$. The height, h, and radius, r, of the cylindrical module are constrained to the given fixed numbers yielding the linear and the quadratic constraint in the variable $\mathbf{p}_1$,

$$\begin{bmatrix} 0 & 0 & 1 \end{bmatrix} (\mathbf{p}_2 - \mathbf{p}_1) = h, \quad \mathbf{p}_1^T \begin{bmatrix} 1 & 0 & 0 \\ 0 & 1 & 0 \\ 0 & 0 & 0 \end{bmatrix} \mathbf{p}_1 = r^2. \tag{31}$$

The nodal displacement constraint is defined to reflect the fact that the bottom nodes of the module are attached to the fixed supports. An equivalent formulation of the yield strength constraint may be obtained by

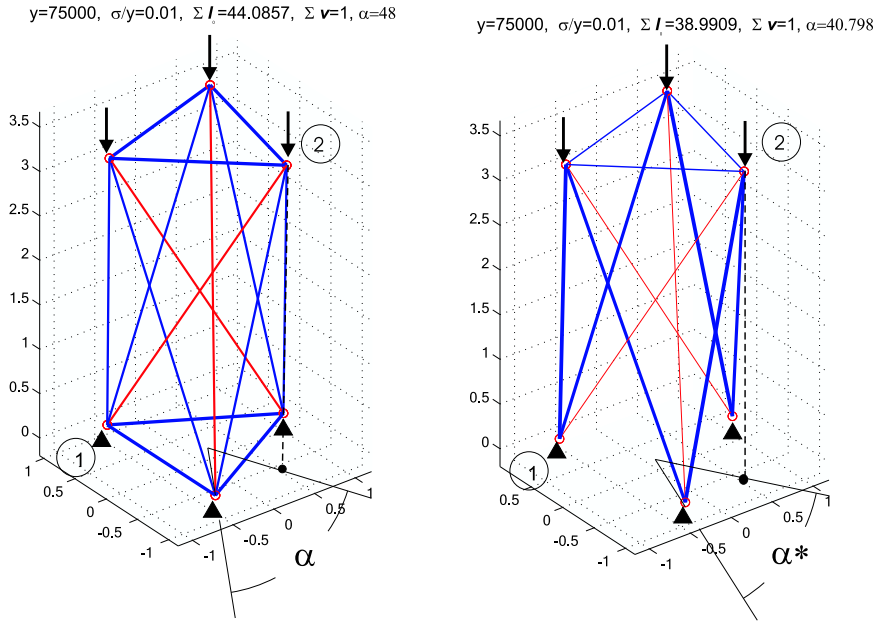

Figure 2. Initial (left) vs. optimal (right) geometry of the structure for one choice of the material parameters when the strength constrains for the loaded configuration are not imposed

dividing it with the Young's modulus y. Hence, material yield stress, σ, is substituted in the problem with the material strength–to–elasticity ratio, σ/y, (yield strain), that modifies the direction of the constraint Jacobian. Increasing the value of the σ/y ratio effectively makes the yield stress constraint less restrictive compared to other constraints. Smaller values of this parameter correspond to rubber–like materials that can undergo large elastic deformation, whereas the large ratio, σ/y, pertains to more traditional, metal–like engineering materials. This problem was solved for several different choices of the material parameters y and σ/y in order to investigate their influence on the optimal topology while keeping the applied load constant. In order to make these results comparable to the stiffness optimization methods that do not take strength constraints into account, a separate

problem is solved where the strength constraints of the loaded structure were relaxed. These constraints for the unloaded structure remained imposed in order to limit otherwise unbounded stiffening effect of the prestress. The presence of this effect can be verified by inspecting the stiffness matrix of a prestressed structure given in [14]. Optimal values of the resulting module twist angle, α, for different choices of material parameters and different active strength constraints are given in Figure 3.

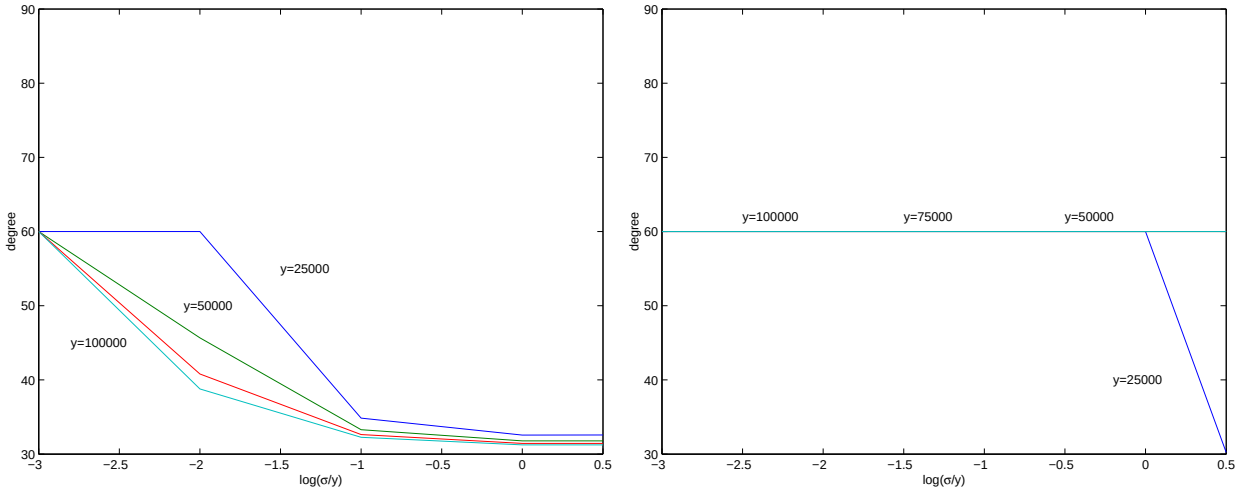

Figure 3. Optimal twist angle of the three–bar unit vs. material parameters: left: without imposing strength and buckling constraints for the loaded configuration; right: with strength and buckling constraints for the loaded configuration

5. DISCUSSION

The results shown in Figure 3 indicate that $\alpha = 60^o$ is the optimal twist angle of the three–bar module for most materials when the strength constraints of the loaded structure are applied and that it is very insensitive to the material parameters variation. This angle lies in the middle of the feasible range for the three–bar module as shown in [27].

In the case when strength constraints of the loaded structure are relaxed, this angle converges to 30^o as the material strength–to–stiffness ratio increases. It may seem to be a paradox that this angle converges to the value at which, the linearized stiffness matrix of a structure exhibits rank deficiency if the structure is not prestressed, indicating a presence of an infinitesimal mechanism mode. Our results clearly show that the configuration that would normally be inferior for structures of metal–like materials, are superior for structures of rubber–like materials which can be attributed to a different relative contribution of the prestress to the structure stiffness. In the sequel we try to rationalize this claim.

By inspecting the stiffness matrix of a prestressed structure given in [14] one can show that increasing prestress in a structure increases its stiffness. It can also be realized that the sensitivity of the condition number of the stiffness matrix to this change increases as the material strength–to–elasticity ratio increases. This leads to the conclusion that significant stiffening of a structure due to the prestress may be expected only if the structure is of a material with a relatively high strength–to–elasticity ratio. Most biological materials belong to this category which may explain a noticeable sensitivity of the cytoskeleton stiffness to prestress change as several researchers verified, e.g. [28].

As it is well known some geometric configurations yield superior stiffness properties. Our results indicate that there also exist configurations that enable larger impact of the prestress which in some materials predominantly contributes to the structure stiffness. These results indicate those configurations for the the three–bar tower module.

6. CONCLUSIONS

The increased interest in tensegrity structures requires addressing problems of their structural optimization. Unlike methods that concern finding feasible tensegrity geometries only, this paper proposes a systematic procedure for designing optimal tensegrity structures. Including additional common constraints was an important step toward deriving more advance tensegrity design tools. The choice for the design variables and the way that the constraints are formulated clearly display their interconnections and suggests efficient ways of scaling the constraints to improve efficiency of the numerical optimization algorithms.

One of the novelties introduced in this paper is the utilization of optimization methods for solving nonlinear static response problems associated with large nodal displacements. In addition to a higher accuracy in predicting a static response of a structure, this method enables efficient solutions of the problems in structures that have ill-conditioned or even singular stiffness matrices at no additional cost. It also indirectly incorporates global buckling as a possible mode of the deformation of the structure.

There is no guarantee that the results shown here represent global optimal solutions because of the non-convex nature of the optimization problem. In some instances, repeated solutions increased confidence to draw several general conclusions. This paper demonstrates that,

- optimization of tensegrity topology and geometry, cast in the form of the nonlinear program, is effectively solvable, and
- if the problem is feasible, the optimization approach is an appropriate design tool that guarantees a monotonic stiffness improvement compared to the initial design.

REFERENCES

1. R. E. Skelton and R. Adhikari. An introduction to smart tensegrity structures. In *Proc. 12th ASCE Engineering Mechanics Conf.*, pages 24–27, San Diego, CA, USA, March, 1998.
2. M. Masic and R.E. Skelton. Path planing and open-loop shape control of modular tensegrity structures. *AIAA Journal of Guidance, Control, and Dynamics-submitted 12-03-2003.*
3. R. E. Skelton, J.P. Pinaud, and D.L. Mingori. Dynamics of the shell-class tensegrity structures. *Journal of The Franklin Institute*, 2-3(338), 2001.
4. C. Sultan and R.E. Skelton. Integrated design of controllable tensegrity structures. In *Proceedings of the ASME International Congress and Exposition 54*, pages 27–37, 1997.
5. C. Sultan and R.E. Skelton. Force and torque smart tensegrity sensor. In *Proceedings of SPIE* 5^{th} *Symposium on Smart Structures and Materials 3323*, pages 357–368, 1998-1.
6. C. Sultan and R.E. Skelton. Tendon control deployment of tensegrity structures. In *Proceedings of SPIE* 5^{th} *Symposium on Smart Structures and Materials 3323*, pages 455–466, 1998-2.
7. C. Sultan, M. Corless, and R.E. Skelton. Peak to peak control of an adaptive tensegrity space telescope. In *Proceedings of SPIE* 6^{th} *Symposium on Smart Structures and Materials 3323*, pages 190–201, 1999.
8. C. Sultan, M. Corless, and R.E. Skelton. Tensegrity flight simulator. *Journal of Guidance, Control, and Dynamics*, 23(6):1055–1064, 2000.
9. C. Sultan, M. Corless, and R. E. Skelton. Symmetric reconfiguration of tensegrity structures. *International Journal of Solids and Structures*, 39:2215–2234, 2002.
10. S. Pellegrino and C.R. Calladine. Matrix analysis of statistically and kinematically indeterminate frameworks. *International Journal of Solids and Structures*, 22(4):409–428, 1985.
11. S. Pellegrino. Foldable bar structures. *International Journal of Solids and Structures*, 34(15):1825–1847, 1997.
12. R. Motro. Tensegrity systems: The state of the art. *International Journal of Space Structures*, 7(2):75–83, 1992.
13. A. Hanaor. Double-layer tensegrity grids - static load response. 1. analytical study. *Journal of Structural Engineering-ASCE*, 117(6):1660–1674, 1991.

14. M. Masic, R.E. Skelton, and P. Gill. Algebraic tensegrity form-finding. *International Journal of Solids and Structures-submitted 11-07-2003*.
15. R. Connelly and W. Whiteley. Second order rigidity and prestress stability for tensegrity frameworks. *SIAM Journal of Discrete Mathematics*, 9:453–491, 1996.
16. M. Save, W. Prager, and G. Sacchi. *Structural Optimization, Volume 1, Optimality Criteria,Mathematical Concepts and Methods in Science and Engineering*, volume 34. New York: Plenum Press.
17. G.I.N. Rozvany. *Structural Design via Optimality Criteria,The Prager Approach to Structural Optimization*, volume 8. Dordrecht: Kluwer Academic Publishers.
18. A. R. Diaz and M. P. Bendsoe. Shape optimization of structures for multiple loading conditions using a homogenization method. *Structural Optimization*, 4:17–22, 1992.
19. A. Ben-Tall and M.P. Bendsoe. A new method for optimal truss topology design. *Siam J. Optim*, (3):322–358, 1993.
20. M. P. Bendsoe and N. Kikuchi. Generating optimal topologies in structural design using a homozenization method. *Computer Methods in Applied Mechanics and Engineering*, 71:197–224, 1988.
21. M. P. Bendsoe. Optimal shape design as a material distribution problem. *Structural Optimization*, 1:193–202, 1989.
22. M. P. Bendsoe. *Optimization of Structural Topology, Shape, and Material*. Springer, 1995.
23. A. Ben-Tal, M. Kočvara, A. Nemirovski, and J. Zowe. Free material design via semidefinite programming: The multiload case with contact conditions. *SIAM J. Optimization*, 9:813–832, 1999.
24. A. Ben-Tal and A. Nemirovski. Robust truss topology design via semidefinite programming. *SIAM J. Optimization*, 7:991–1016, 1997.
25. F. Jarre, M. Kocvara, and J. Zowe. Optimal truss design by interior-point methods. *Siam J. Optim*, 8(4):1084–1107, 1998.
26. P. E. Gill, W. Murray, and M. A. Saunders. User's guide for SNOPT 5.3: a Fortran package for large-scale nonlinear programming. Numerical Analysis Report 97-5, Department of Mathematics, University of California, San Diego, La Jolla, CA, 1997.
27. M. Masic and R.E. Skelton. Open–loop control of class–2 tensegrity towers. In *Proceedings of the SPIE 11th Annual International Symposium on Smart Structures and Materials*.
28. D. Stamenovic, J.J. Fredberg, N. Wnag, J.P. Butler, and D.E. Ingber. A microstructural approach to cytoskeletal mechanics based on tensegrity. *Journal of Theoretical Biology*, 181(2):125–136, 1996.